

Surface-Initiated Polymerization of 2-Hydroxyethyl Methacrylate from Heterotelechelic Oligoperoxide-Coated γ -Fe₂O₃ Nanoparticles and their Engulfment by Mammalian Cells

Daniel Horák,^{*,†} Tetiana Shagotova,[†] Nataliya Mitina,[‡] Miroslava Trchová,[†] Nataliya Boiko,[§] Michal Babič,[†] Rostyslav Stoika,[§] Jana Kovářová,[†] Orest Hevus,[‡] Milan J. Beneš,[†] Olga Klyuchivska,[§] Petr Holler,[†] and Alexander Zaichenko[‡]

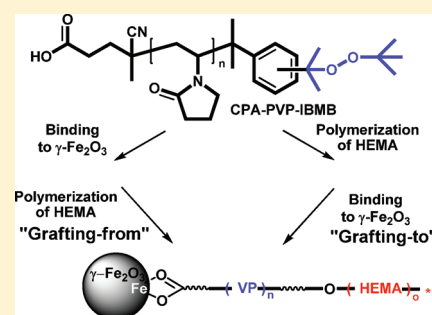
[†]Institute of Macromolecular Chemistry AS CR, Heyrovského Sq. 2, 162 06 Prague 6, Czech Republic

[‡]Lviv Polytechnic National University, St. Bandery 12, 79 013 Lviv, Ukraine

[§]Institute of Cell Biology NASU, Dragomanov St., 14/16, 79005, Lviv, Ukraine

ABSTRACT: Novel heterotelechelic poly(*N*-vinylpyrrolidone) (CPA-PVP-IBMB) oligoperoxide containing anchoring carboxyl group from 4-cyanopentanoic acid (CPA) and peroxide end-group from 1-isopropyl-3(4)-[1-(tert-butyl peroxy)-1-methylethyl]benzene (IBMB) chain transfer agent was synthesized and investigated as a surface-active macroinitiator for tailored functionalization of maghemite (γ -Fe₂O₃) nanoparticles. CPA-PVP-IBMB initiated polymerization of 2-hydroxyethyl methacrylate (HEMA) in ethanol yielding CPA-PVP-*block*-poly(2-hydroxyethyl methacrylate) (CPA-PVP-*block*-PHEMA) copolymer. γ -Fe₂O₃ nanoparticles obtained by precipitation technique were modified by the CPA-PVP-IBMB macroinitiator and CPA-PVP-*block*-PHEMA copolymer by “grafting-to” approach to the surface using carboxyl end groups of both polymers. Second method, “grafting-from” approach, consisted in polymerization of HEMA initiated from the surface of CPA-PVP-IBMB-coated γ -Fe₂O₃ nanoparticles yielding CPA-PVP-IBMB-coated γ -Fe₂O₃/PHEMA nanoparticles. Tests with mice leukemia L1210 cells confirmed nontoxicity of CPA-PVP-IBMB-coated γ -Fe₂O₃/PHEMA nanoparticles. CPA-PVP-IBMB-coated γ -Fe₂O₃/PHEMA nanoparticles were easily engulfed by murine macrophages J774.2 and magnetically separated from cells without phagocytic activity.

KEYWORDS: 2-hydroxyethyl methacrylate, oligoperoxide, surface-initiated polymerization, magnetic, nanoparticles, macrophage, cell engulfment



INTRODUCTION

Magnetic nanoparticles have passed through rapid development within the last 30 years. They found manifold applications, from sealing ferrofluids^{1,2} to today's use in biotechnology and biosciences.^{3–5} This includes magnetic separations,^{6–8} sensors,^{9–11} drug and gene delivery,^{12–15} hyperthermia,^{16,17} and contrast enhancement in magnetic resonance imaging (MRI).^{18–21} Magnetic nanoparticles are mostly based on iron oxide, which has been approved by FDA as an MRI contrast agent²² and has the advantage of being biocompatible, nontoxic, and nonimmunogenic. The nanoparticles are generally composed of the magnetic core, water-dispersible biocompatible shell, and a target biomolecule.

The choice of the synthesis method is of key importance because it determines the nanoparticle shape and size as well as its size distribution and surface chemistry. Magnetic nanoparticles are typically synthesized by a coprecipitation route or by thermal decomposition of iron pentacarbonyl and iron acetylacetonate.²³ However, their drawback consists in nonspecific adsorption of proteins from the media and easy aggregation which prevents their direct applications. For the magnetic iron oxide nanoparticles to be used, i.e., dispersed in aqueous

solutions avoiding aggregation, they have to be coated with hydrophilic compounds to stabilize them sterically or electrostatically. Surface modifications like altering the charge, attached polymers, or proteins will play an important role for various subsequent biomedical applications. Most surface modifications of magnetic nanoparticles used dextran^{24,25} or poly(ethylene glycol) shell because of its biocompatibility and plasma protein resistance.^{26,27} The magnetic core should have reactive groups on the surface enabling the attachment of biologically active molecules and ligands for intended application, e.g., antibody/antigen for separation or enzyme for catalysis. A typical example of a method for embedding magnetic nanoparticles by polymers is a miniemulsion polymerization.^{28–30}

One of the useful methods for coating is to graft polymers onto magnetic nanoparticles, forming core–shell hybrid composites. Two approaches are used to graft polymer chains onto nanoparticles: “grafting-to” and “grafting-from”.³¹ In the “grafting-to” system, end-functionalized polymers react with surface

Received: February 9, 2011

Revised: April 19, 2011

Published: May 02, 2011

groups of nanoparticles. In the “grafting-from” method (also called surface-initiated polymerization), polymer chains grow in situ from initiators that have been anchored to the surface of the nanoparticles. Higher grafting density can be achieved because the smaller monomers are accessible to the active initiation sites.^{32,33} The methods include surface-initiated anionic,³⁴ cationic,^{35–37} or ring-opening polymerization for coating with biodegradable polyesters or hyper-branched polymers.^{38–42} Other techniques, such as ring-opening metathesis polymerization^{43,44} and controlled living radical polymerizations including atom-transfer radical polymerization,^{45–47} nitroxide-mediated controlled polymerization,⁴⁸ and reversible addition–fragmentation chain transfer,⁴⁹ have been utilized for introduction of reactive polymer spacers. Tailored synthesis of novel oligoperoxide surfactants containing peroxide or hydroperoxide side groups and their application for functionalization of nanoparticle surface and subsequent initiation of the polymerization^{50–53} provides a new perspective route for obtaining functional magnetic nanoparticles for biomedical applications. This approach provides covalent attachment of functional biocompatible spacers of desired length with peroxide end-fragments capable of radical formation for subsequent tailored functionalization of maghemite (γ -Fe₂O₃) nanoparticles. This makes binding enzymes, antibodies, drugs, DNA, and oligonucleotides possible.

The purpose of this study is to take advantage of a new heterotelechelic macroinitiator^{54,55} containing a carboxyl end-group for the attachment to iron oxide surface,⁵⁶ polyvinylpyrrolidone chain to introduce hydrophilicity and biocompatibility,⁵⁷ and a peroxide end-group capable of initiating a polymerization both by “grafting-from” and “grafting-to” approach. The maghemite nanoparticles modified with the block copolymer originating from the heterotelechelic initiator were then tested for engulfment of J774.2 murine macrophages and their magnetic separation. Measurement of phagocytic capacity is one of the most common methods to evaluate immune status of the patient, namely the activity of blood leukocytes. It is used in diagnostics of various pathological states. Neutrophils and macrophages are the main types of the immune cells targeting microorganisms, impaired cells and foreign antigens. Phagocytosis starts from recognizing these foreign objects, their engulfment and destruction. Phagocytic activity is typically measured by calculating the number of engulfed objects under the microscope or by flow cytometry.

EXPERIMENTAL SECTION

Materials. 1-Vinyl-2-pyrrolidone (VP) was from ABCR (Karlsruhe, Germany), 4,4'-azobis(4-cyanopentanoic acid) (ACPA) and 2,2-diphenyl-1-picrylhydrazyl (DPPH) were from Aldrich (Milwaukee, WI, USA). 1-Isopropyl-3(4)-[1-(*tert*-butyl peroxy)-1-methylethyl]benzene (IBMB) was synthesized from *tert*-butyl hydroperoxide (9.9 g, 110 mmol) and 2-(4-isopropylphenyl)-2-propanol (17.8 g, 100 mmol) in acetic acid solution as described earlier.^{58,59} Obtained oligoperoxide was purified by distillation in vacuum. Yield 82%. Bp 69 °C (10 Pa). d_4^{20} 0.9208. n_D^{20} 1.4811. Found, %: C 76.64; H 10.57; O_{act} 6.3. C₁₆H₂₆O₂. Calculated, %: C 6.73; H 10.48; O_{act} 6.39. ¹H NMR (CDCl₃), δ , ppm: 1.16 s (9H, (CH₃)₃C); 1.45 s (6H, C(CH₃)₂Ph); 7.05 dd (4H, Ar-H); 1.17 d (6H, (CH₃)₂CH); 2.77 hp (1H, (CH₃)₂CH). Meso-2,3-dimercaptosuccinic acid (DMSA) and mercaptosuccinic acid (MSA) were from Aldrich, ethyl acetate, acetone and hexane were purchased from Merck (Darmstadt, Germany), other solvents and reagents were obtained from Aldrich. Acetonitrile was from Lach-Ner (Neratovice, Czech Republic). Ultrapure Q water ultrafiltered on a Milli-Q Gradient A10

Table 1. Chemical Properties of CPA-PVP-IBMB Macroinitiator

C (wt %)	N ^a (wt %)	VP ^a (mmol/g)	COOH (mmol/g)	C in CPA ^b (wt %)	C in IBMB ^c (wt %)	IBMB (mmol/g)
57.1	10.5	7.5	0.25	0.5	2.5	0.33

^a On the basis of nitrogen analysis. ^b %C in residue after decomposition of CPA in CPA-PVP-IBMB calculated from mmol COOH/g (determined from titration). ^c %C in IBMB = 57.1 – 54.1 – 0.5, where 54.1% is %C in PVP calculated from nitrogen content.

Table 2. Chemical Properties of CPA-PVP-*block*-PHEMA Obtained by CPA-PVP-IBMB-Initiated Polymerization of HEMA

CPA-PVP-IBMB/ HEMA (w/w)	N (wt %)	VP ^a (wt %)	M _n ^b (Da)	PI ^c
1/1	6.8	51	35 400	2.15 ^b
1/2	3.8	30	42 100	2.94 ^b
1/5	2.8	23	>150 000	^d
1/10	2.15	17	>200 000	^d

^a On the basis of nitrogen analysis. ^b Determined from SEC. ^c Dispersity. ^d Not determined.

system (Millipore, Molsheim, France) was used for preparation of solutions.

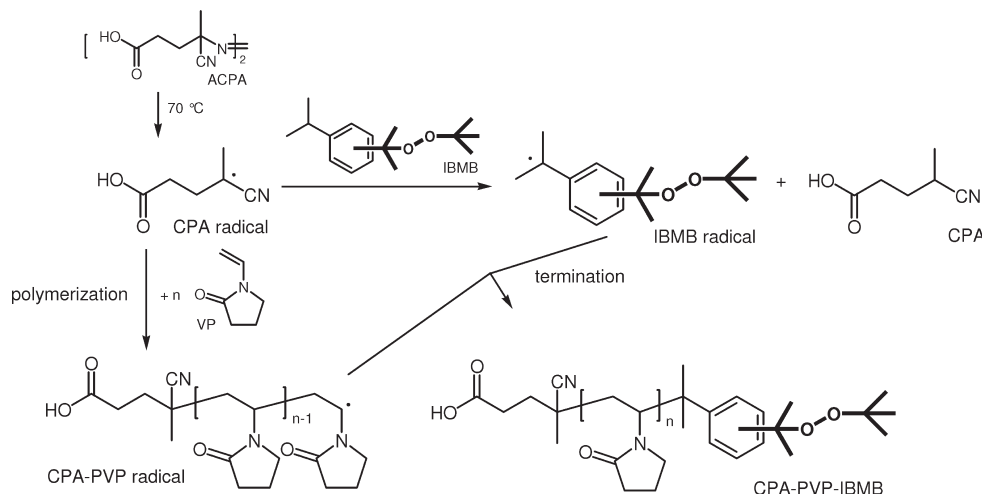
Synthesis of CPA-PVP-IBMB Macroinitiator. The synthesis was described earlier.⁵⁸ In a typical experiment, ACPA (0.39 g; 2 mmol) was dissolved in ethyl acetate (15 mL), VP (12.45 g; 112 mmol) and IBMB (7.6 g; 30 mmol) were added and the mixture was purged with argon. Polymerization proceeded at 70 °C for 6 h under argon atmosphere. Conversion was 85% as determined from dilatometer and gravimetric measurements.⁶⁰ After the polymerization, the solution was precipitated by hexane; the CPA-PVP-IBMB macroinitiator was dissolved in acetone (15 mL) and again precipitated in hexane (200 mL). The procedure was repeated three times. Yield was 8.7 g (conversion 70%). Properties of the CPA-PVP-IBMB macroinitiator are listed in Table 1.

Copolymerization of CPA-PVP-IBMB with HEMA. Various amounts of HEMA (Table 2) were added to the solution of CPA-PVP-IBMB (0.45 g) in ethanol (25 mL). The mixture was stirred at 80 °C for 24 h under inert atmosphere, the resulting CPA-PVP-*block*-PHEMA polymer was precipitated from the solution by petroleum ether (400 mL) and dried under vacuum at 40 °C for 8 h. Yield was 1.23 g (conversion 82%) if CPA-PVP-IBMB/HEMA ratio was 1/2 (w/w).

If chain-transfer agents were used in the reaction, DMSA or MSA (0.09 g) was dissolved in ethanolic CPA-PVP-IBMB (0.5 g) solution (25 mL), HEMA (5 g) was added, and the mixture heated at 80 °C for 24 h. Precipitation was done as described above.

Coating of γ -Fe₂O₃ Nanoparticles. Maghemite was prepared according to the method described earlier.⁶¹ CPA-PVP-IBMB macroinitiator (2–340 mg) or CPA-PVP-*block*-PHEMA (5–340 mg) was dissolved in γ -Fe₂O₃ colloid (10 mL; 170 mg of nanoparticles) at 23 °C and stirred for 1 h. The product was purified by repeated washing (five times) with water (20 mL) using magnetic separation.

Surface-Initiated Polymerization of HEMA on CPA-PVP-IBMB-Coated γ -Fe₂O₃ Nanoparticles. As an example, HEMA (80 mg) was dissolved in CPA-PVP-IBMB-coated γ -Fe₂O₃ colloid (10 mL; CPA-PVP-IBMB/ γ -Fe₂O₃ ratio = 8/170 w/w), the mixture was stirred at 80 °C for 24 h under nitrogen atmosphere, and the sediment was washed five times with water (10 mL each) and dried.

Scheme 1. ACPA-Initiated Polymerization of VP in the Presence of IBMB Chain Transfer Agent^a

^aIBMB is a mixture of 1-isopropyl-3-[1-(*tert*-butyl peroxy)-1-methylethyl]benzene and 1-isopropyl-4-[1-(*tert*-butyl peroxy)-1-methylethyl]benzene.

Characterization. ¹H and ¹³C NMR spectra were recorded on a Bruker Avance DPX 300 spectrometer at 300.13 and 75.45 MHz, respectively. Polymer molecular weights were estimated using size-exclusion chromatography (SEC) with a LCP 4020 pump (Ecom, České Meziříčí, Czech Republic), a Shodex 602 column (Kawasaki, Japan) and a RIDK 101 refractive index detector (Laboratorní přístroje, Prague, Czech Republic). *N,N*-dimethylacetamide with LiBr addition was used as a mobile phase at flow rate 1 mL/min and polystyrene standards for calibration. The hydrodynamic diameter (*z*-average) and the surface zeta-potential were obtained by dynamic light scattering (DLS) with an Autosizer Lo-C (Malvern Instruments Ltd., Malvern, Great Britain). Original dispersion of the nanoparticles (0.1 mL aliquot) was diluted with Q water (1 mL) before the measurement.

The molecular weights of CPA-PVP-IBMB macroinitiator and CPA-PVP-*block*-PHEMA copolymer were determined by System ALV static light scattering apparatus (Langn, Germany) from angle- and concentration-dependences of the intensity of scattered light, using a Zimm plot.

Infrared spectra were measured using a Thermo Nicolet NEXUS 870 FTIR Spectrometer (Madison, WI, USA). Golden Gate Heated Diamond ATR Top-Plate (MKII Golden Gate single reflection ATR system) (Specac Ltd., Orpington, Great Britain) was applied for the measurements of spectra of the powdered samples.

The iron content was analyzed by a Perkin-Elmer 3110 (Norwalk, CT, USA) atomic absorption spectrometer (AAS) using a solution obtained by mineralization of a sample with dilute HCl (1:1) at 80 °C for 1 h. Elemental analysis was performed on a Perkin-Elmer 2400 CHN elemental analyzer. Content of COOH groups was determined by titration of the polymer (0.3 g) in 0.1 N NaOH solution (15 mL). The relative content of polymer and Fe₂O₃ were determined using a Perkin-Elmer TGA 7 Thermogravimetric Analyzer (Norwalk, CT, USA). The sample was heated from room temperature to 800 °C at a heating rate of 10 °C/min under air.

The iron oxide particles were observed in a Tecnai Spirit G2 transmission electron microscope (TEM; FEI, Brno, Czech Republic). A drop of particle dispersion (20 μL) on Cu grid was coated with a carbon film. The number-average diameter (*D_n*) and particle-size distribution PDI (weight-to-number-average particle diameter *D_w*/*D_n*) were obtained by statistical treatment of at least 500 particles using program Atlas (Tescan, Brno, Czech Republic).

To confirm the presence of peroxides in CPA-PVP-IBMB macroinitiator, DPPH (30 mg) was dissolved in *N,N*-dimethylformamide (50 mL), which was purged with nitrogen for 30 min, and CPA-PVP-

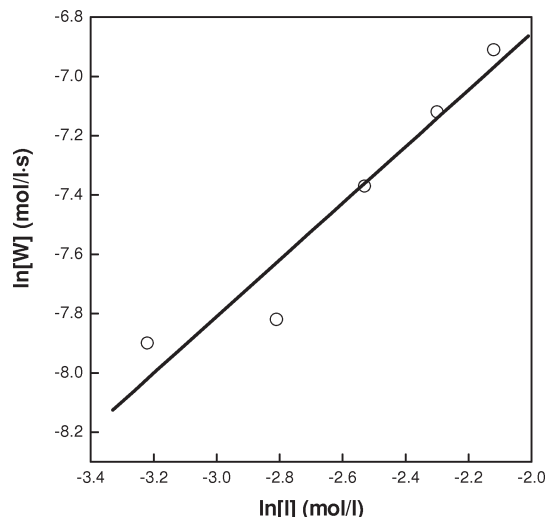


Figure 1. Dependence of rate of VP polymerization in the presence of IBMB chain-transfer agent on ACPA initiator concentration.

IBMB (340 mg) was added. The mixture was heated for 10 min at 80 °C and after cooling UV spectrum (520 nm) of the solution was recorded on a Lambda 20 Perkin-Elmer UV/VIS spectrometer (Norwalk, CT, USA). Analogously, UV spectrum of DPPH solution was measured as a check.

Reaction order of ACPA initiator in the concentration range 0.04–0.12 mol/L was determined under constant concentrations of all other reaction components.⁶²

Cell Experiments. *Cell Culture.* Murine macrophages of J774.2 line and leukemia cells of L1210 line were obtained from William Harvey Institute (London, U.K.) and cultured in Dulbecco's-modified Eagle's medium (DMEM; Sigma, St. Louis, USA) supplemented with 10% fetal bovine serum (FBS; Sigma). Cells were kept in CO₂ incubator at 37 °C, 5% CO₂, and 100% humidity.

Oposonization of CPA-PVP-IBMB-Coated γ-Fe₂O₃/PHEMA Nanoparticles and Their Phagocytosis by the Macrophages. The CPA-PVP-IBMB-coated γ-Fe₂O₃/PHEMA nanoparticles were opsonized at 37 °C for 24 h with proteins of the FBS used for cell culturing. The opsonized particles were added to a suspension of the macrophages J774.2 (final

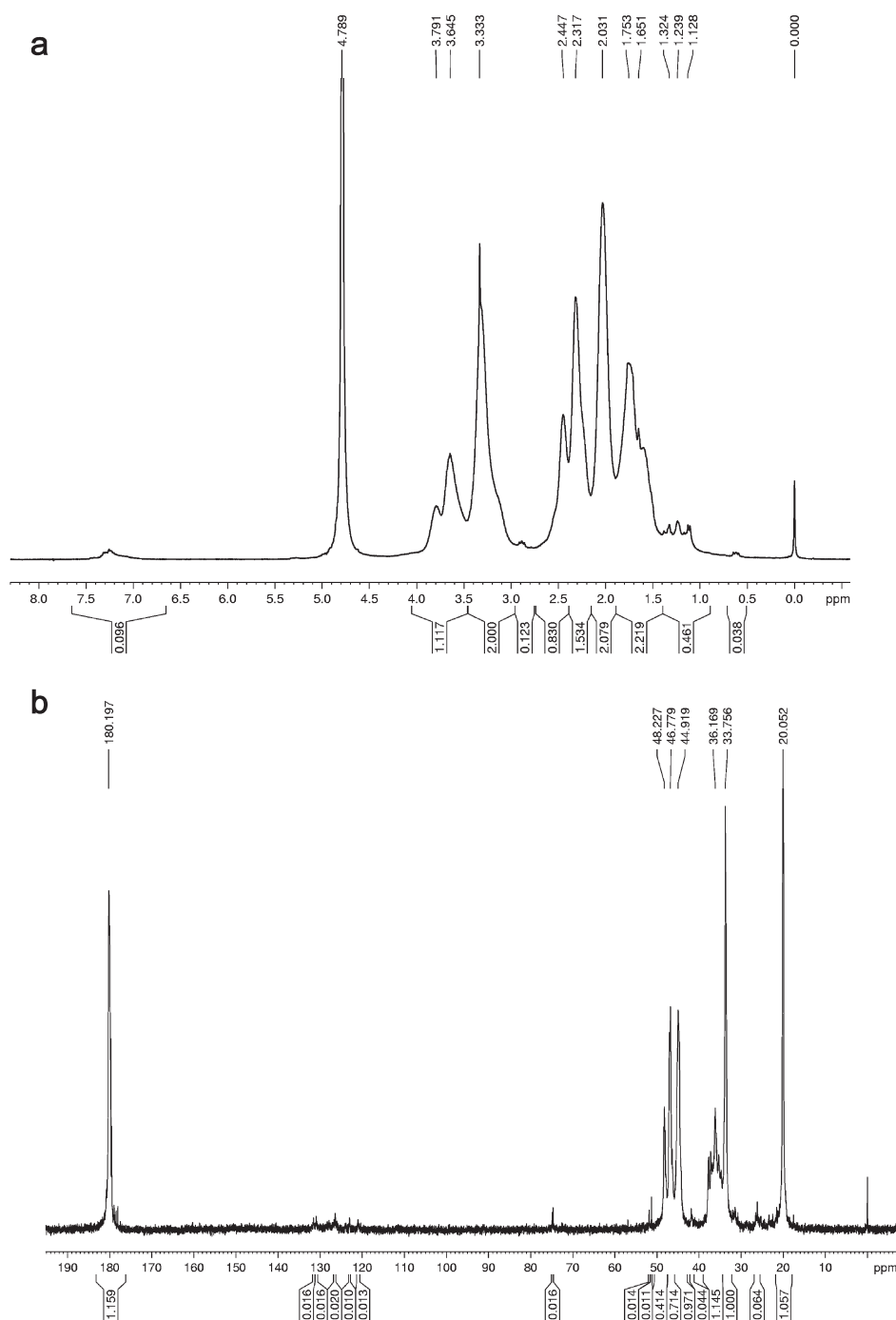


Figure 2. (a) ^1H and (b) ^{13}C NMR spectra of CPA-PVP-IBMB macroinitiator in (a) D_2O and (b) methanol.

concentration of the particles 0.025 wt %) and the culture was kept in CO_2 incubator for 24 h until the particles were phagocytosed. Phagocytosis-positive and phagocytosis-negative macrophage fractions were then separated by the Dynal MPCTM-1 magnet. The macrophages that engulfed the superparamagnetic particles were attracted by the magnet, whereas the particle-free macrophages remained in the culture medium. Phagocytosis of neat $\gamma\text{-Fe}_2\text{O}_3$ nanoparticles by the macrophages was used as a control.

Light and Fluorescence Microscopy. Cell fractions were stained with acridine orange and Hoechst 33342 and then observed and photographed under Carl Zeiss AxioImager A1 light and fluorescent microscope. Final concentration of both dyes was $0.3\ \mu\text{g}/\text{mL}$ and staining time 15 min. Excitation was at 365–395 nm and emission at 445–450 nm for

Hoechst 33342. For acridine orange, excitation and emission was at 470–495 nm and 525–550, respectively, with green filter and at 546–560 and 575–640 nm, respectively, with red filter.

Cytotoxicity of CPA-PVP-IBMB-coated $\gamma\text{-Fe}_2\text{O}_3$ /PHEMA nanoparticles was estimated by counting the number of murine leukemia L1210 cells in the presence of particles (0.025, 0.5, and 1 wt %) in DMEM medium in the hemocytometric chamber after 24 and 48 h cultivation.

RESULTS AND DISCUSSION

CPA-PVP-IBMB Macroinitiator. CPA-PVP-IBMB macroinitiator was prepared by the ACPA-initiated solution polymerization

of VP in ethyl acetate in the presence of IBMB acting as a chain-transfer agent according to the published procedure⁵⁸ (Scheme 1). Reaction started by the decomposition of ACPA forming relatively stable radicals which participated in the termination of growing PVP chains under formation of CPA-PVP-IBMB macroinitiator (Scheme 1). The reaction order on ACPA initiator approached 1 (Figure 1) confirming thus that the proposed mechanism of heterotelechelic oligoperoxide formation (Scheme 1). The structure of the CPA-PVP-IBMB in D₂O and methanol-*d*₃ was confirmed by ¹H and ¹³C NMR, respectively (Figure 2 a, b). In ¹H NMR, the VP units offered the following signals: skeletal CH₂ at 1.239 ppm, skeletal CH at 3.645 and 3.791 ppm; pyrrolidone ring: α-CH₂ 3.333 ppm, β-CH₂ 2.031 ppm, γ-CH₂ at 2.317 and 2.447 ppm (Figure 2 a). In ¹³C NMR: skeletal CH₂ at 44.919 ppm, skeletal CH at 48.227 ppm; pyrrolidone ring: α-CH₂ 46.779 ppm, β-CH₂ 20.052, γ-CH₂ 33.756 and C=O 180.197 ppm (Figure 2 b). ¹H and ¹³C NMR spectra of CPA-PVP-IBMB thus confirmed presence of VP units in the polymer (Figure 2 a, b). Quaternary carbons at 74 ppm in ¹³C NMR spectrum and benzene ring carbons at 7.2 ppm and at 130 ppm in ¹H NMR and ¹³C spectrum, respectively, indicated presence of peroxide. Because of low CPA content in the macroinitiator, decrease of the UV signal at 520 nm was only moderate. The content of carboxyl end-groups in CPA-PVP-IBMB macroinitiator determined by titration increased and at the same time molecular weight decreased with increasing concentration of ACPA in initial monomer mixture (Table 3).

According to the NMR spectrum, the CPA-PVP-IBMB macroinitiator contained 150 VP units, i.e., its molecular weight *M_n* was 17 000 Da. This was in agreement with the measurement of molecular weight by the size-exclusion chromatography (SEC) in *N,N*-dimethylacetamide, where *M_n* = 18 000 and dispersity = 1.74 were determined, even though the PS standards were used for the calibration, which differed from PVP in polarity. The presence of a single peak of the CPA-PVP-IBMB macroinitiator in the SEC chromatogram indicated that heterotelechelic PVP peroxide was formed predominantly. Determination of molecular weight by SEC was in agreement with the measurement of molecular weight by the static light-scattering in methanol (*M_w* ~ 17,000 Da) and viscosimetry. According to elemental analysis and titration, the CPA-PVP-IBMB macroinitiator contained approximately 10.5 wt % nitrogen (7.51 mmol VP/g), 0.25 mmol COOH/g originating from ACPA initiator and 0.33 mmol IBMB/g (Table 1). Ratio of anchoring COOH groups/VP units/aromatic peroxide end-groups of CPA-PVP-IBMB macroinitiator was thus 1/30/1.3 (mol/mol/mol), respectively (Table 1). The amount of VP in the macroinitiator was thus lower than that according to the NMR spectrum. This discrepancy can be ascribed to branching of the polymer chain and/or to the error caused by combustion of inhomogeneous samples during the analysis.

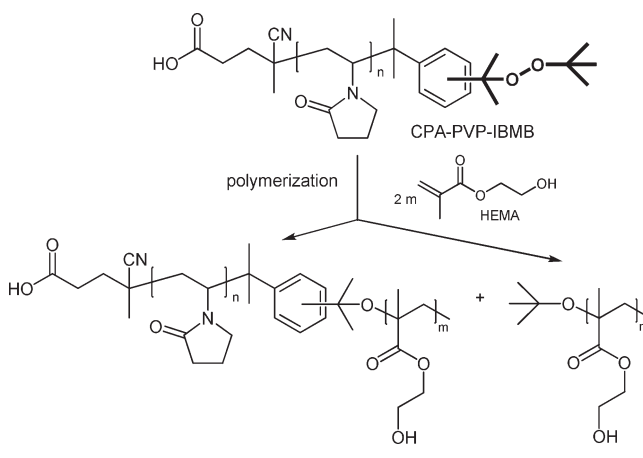
To determine presence of the peroxide in the CPA-PVP-IBMB macroinitiator, we have reacted 2,2-diphenyl-1-picrylhydrazyl (DPPH) with free radicals formed by splitting of CPA-PVP-IBMB at elevated temperature (80 °C) in DMF, resulting in nonreactive products.⁶³ The decrease in DPPH concentration in the presence of CPA-PVP-IBMB macroinitiator in the UV spectrum reflected the decomposition of CPA-PVP-IBMB. Peroxide end-group of CPA-PVP-IBMB macroinitiator is intended to initiate polymerization of HEMA either in ethanolic solution or on the surface of magnetic nanoparticles.

Table 3. Effect of ACPA Concentration on the Content of Carboxyl Groups and Molecular Weight of CPA-PVP-IBMB Macroinitiator^a

concentration of ACPA in feed (mol/L)	CPA-PVP-IBMB		
	COOH content (wt %)	[η] (g/L)	<i>M_n</i> (kDa)
0.04	1.11	0.3058	59
0.06	1.09	0.2050	31
0.08	1.35	0.1475	21
0.10	1.85	0.1333	18
0.12	2.67	0.1255	17

^a Intrinsic viscosity [η] = 1.4 × 10⁻⁴ M^{0.7}; *M_n* = number molecular weight; H₂O, 25 °C.

Scheme 2. Copolymerization of CPA-PVP-IBMB with HEMA



CPA-PVP-IBMB-Initiated Polymerization of HEMA. HEMA was intentionally selected for CPA-PVP-IBMB-initiated polymerization because its polymer is a neutrally charged hydrogel, biocompatible, biologically inert and highly resistant to protein adsorption and consequently cell adhesion,⁶⁴ and containing hydroxyl groups which can be used for attachment of biomolecules. It is attractive, because its mechanical properties can be tailored to the specific application. Copolymers of VP and HEMA with various compositions can be obtained with well-defined properties. The effects of different block copolymers on the characteristics of maghemite nanoparticles were examined. Moreover, insolubility of PHEMA in water belongs to its advantage, because it favors its sticking on the iron oxide surface hindering release from the particles. HEMA was thus solution polymerized with CPA-PVP-IBMB macroinitiator in ethanol yielding CPA-PVP-*block*-PHEMA copolymer (Scheme 2). If CPA-PVP-IBMB/HEMA ratio was 1/2 (w/w), SEC of the resulting CPA-PVP-*block*-PHEMA product in *N,N*-dimethylacetamide revealed a broad and unimodal peak corresponding to *M_n* = 42 000 Da and dispersity = 2.94, i.e., both the molecular weight and dispersity were higher than in CPA-PVP-IBMB macroinitiator. Moreover, 2.15 wt % nitrogen was found in the CPA-PVP-*block*-PHEMA copolymer suggesting that it contained 17 wt % PVP and 83 wt % PHEMA (Table 4). ATR FTIR spectrum of CPA-PVP-*block*-PHEMA copolymer (its peaks are marked in

Table 4. Chemical Properties of CPA-PVP-*block*-PHEMA Obtained by CPA-PVP-IBMB-Initiated Polymerization of HEMA in the Presence of MSA and DMSA (CPA-PVP-IBMB/HEMA Ratio = 1/10 w/w)

run	CTA ^a (wt %)	C (wt %)	N (wt %)	VP ^b (wt %)	M _n ^c (Da)	PI ^d
CPA-PVP- <i>block</i> -PHEMA-1	0	55.5	2.2	17	>200 000	^e
CPA-PVP- <i>block</i> -PHEMA-2	2 ^f	54.9	1.5	12	23 500	1.83
CPA-PVP- <i>block</i> -PHEMA-3	2 ^g	54.5	1.1	9	20 300	1.85

^aCTA, chain transfer agent. ^bOn the basis of nitrogen analysis. ^cDetermined from SEC. ^dDispersity. ^eNot determined. ^fDMSA, dimercaptosuccinic acid. ^gMSA, mercaptosuccinic acid.

Figure 3) was not only a mix of the spectrum of neat CPA-PVP-IBMB macroinitiator and of neat HEMA but it was very close to the spectrum of neat PHEMA (Figure 3). Besides the peaks of PHEMA at 1721, 1444, 1269, 1152, and 1074 cm⁻¹, the second maximum at about 1656 cm⁻¹ observed in the spectrum of CPA-PVP-*block*-PHEMA belonged to CPA-PVP-IBMB. This signified the formation of CPA-PVP-*block*-PHEMA copolymer.

Several CPA-PVP-IBMB/HEMA ratios were investigated in the CPA-PVP-IBMB-initiated polymerization of HEMA (Table 2). With increasing CPA-PVP-IBMB/HEMA ratio from 1/10 to 1/1 (w/w) (Table 2), content of PVP in the CPA-PVP-*block*-PHEMA copolymer increased from 17 to 51 wt %. At the same time, molecular weight of CPA-PVP-*block*-PHEMA copolymer decreased from 200 000 Da to 35 000 Da according to SEC. The high molecular weight of CPA-PVP-*block*-PHEMA copolymer was also confirmed by the static light-scattering analysis.

To control molecular weight of PVP block and/or to incorporate additional anchoring groups in the copolymer to bind to iron oxide, we investigated the CPA-PVP-IBMB-initiated polymerization of HEMA in the presence of dimercaptosuccinic acid (DMSA) or mercaptosuccinic acid (MSA) as a chain-transfer agent (Table 4). Compared with the polymerization of HEMA in the absence of a chain-transfer agent (resulting M_w = 42 000 Da), presence of DMSA or MSA substantially decreased the molecular weight of the resulting copolymer to 23 500 or 20 300 Da, respectively. According to the elemental analysis, DMSA or MSA induced the decrease of PVP content in CPA-PVP-*block*-PHEMA from 17 wt % to 12 or 9 wt % as more PHEMA was introduced in the resulting copolymer (Table 4).

Advantage of DMSA consists in its high affinity toward the iron oxide surface. The carboxylic acid functionality in CPA-PVP-IBMB and CPA-PVP-*block*-PHEMA polymers provides coordination bond with ferric ions of the iron oxide surface.

Coating of γ -Fe₂O₃ Nanoparticles with CPA-PVP-IBMB Macroinitiator and CPA-PVP-*block*-PHEMA Copolymer. Morphology of the initial γ -Fe₂O₃ nanoparticles and of the CPA-PVP-IBMB and CPA-PVP-*block*-PHEMA-coated nanoparticles was examined by TEM (Figure 4). The average size and polydispersity index of initial nanoparticles were D_n = 11 nm and PDI = 1.15, respectively (Figure 4a). As expected, hydrodynamic diameter from dynamic light scattering (DLS) was substantially larger, 125 nm (Table 5), because of the greater effect of large particles on the hydrodynamic size. DLS provided the z-average of the diameter in water, while TEM gave the number-average of dry particles. Moreover, DLS provided information on the hydrodynamic particle size of whole particle clusters, including polymer coating layers and the magnetic cores. The particles were negatively charged as documented by zeta-potential of -27 mV ensuring colloid stability of the particles.

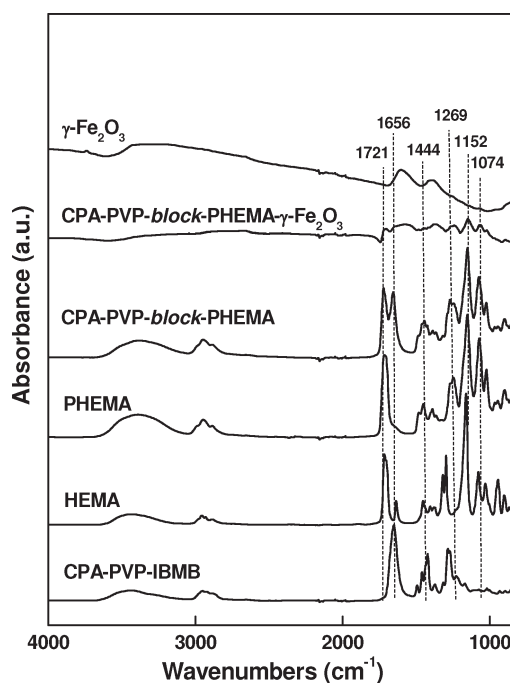


Figure 3. ATR FT-IR spectra of γ -Fe₂O₃ nanoparticles before and after coating with CPA-PVP-*block*-PHEMA; spectra of PHEMA, HEMA, CPA-PVP-IBMB, and CPA-PVP-*block*-PHEMA are shown as a control.

γ -Fe₂O₃ nanoparticles were coated with CPA-PVP-IBMB macroinitiator by the “grafting-to” approach at several CPA-PVP-IBMB/ γ -Fe₂O₃ ratios ranging from 0 to 2 (w/w). It was observed in TEM that after the coating the CPA-PVP-IBMB macroinitiator (CPA-PVP-IBMB/ γ -Fe₂O₃ ratio = 2 w/w) has embedded the 11 nm nanoparticle cores (Figure 4 b). Size of the CPA-PVP-IBMB-coated γ -Fe₂O₃ nanoparticles increased to 19 nm and polydispersity index did not change after the coating (PDI = 1.13). The CPA-PVP-IBMB shell was clearly discernible around the γ -Fe₂O₃ nanoparticles (Figure 4 b). Hydrodynamic diameter of the CPA-PVP-IBMB-coated γ -Fe₂O₃ nanoparticles was 196 nm that is appreciably larger than for initial uncoated nanoparticles. Zeta-potential of the coated nanoparticles (-26 mV) had the same value as that of uncoated particles, which was still sufficient for electrostatic stabilization of the particles (Table 5).

The amount of coating and the content of maghemite in the particles were calculated from percentage of Fe (obtained by AAS). Since CPA-PVP-IBMB does not contain Fe, the percentage of Fe may be used for calculating the percentage of γ -Fe₂O₃ of the CPA-PVP-IBMB-coated γ -Fe₂O₃ nanoparticles according to the following equation: % Fe₂O₃ = (% Fe × 100)/69.75, where % Fe was obtained from AAS and 69.75 was the

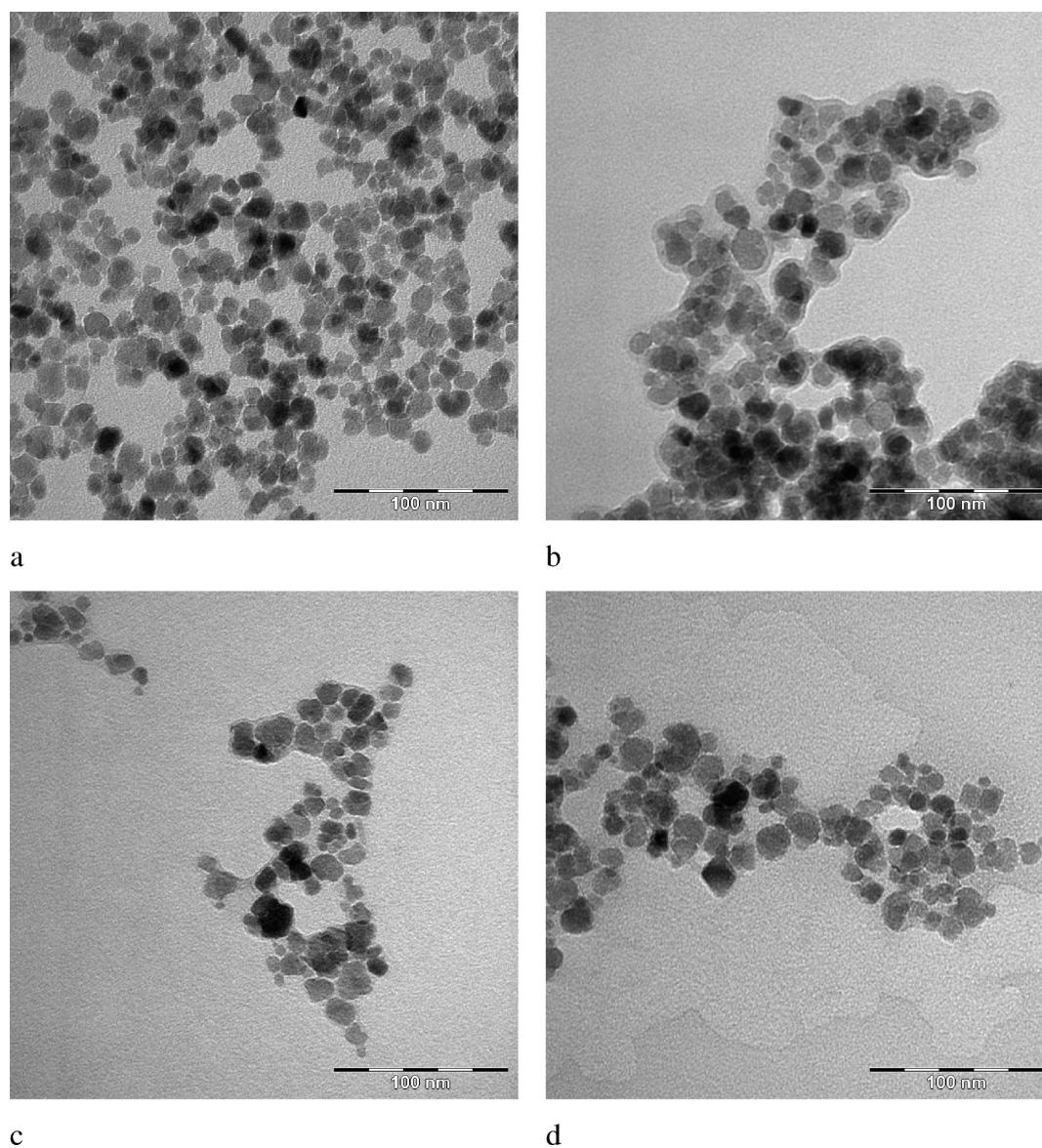


Figure 4. TEM micrographs of (a) γ -Fe₂O₃ nanoparticles synthesized by coprecipitation method, (b) CPA-PVP-IBMB-coated γ -Fe₂O₃, (c) CPA-PVP-*block*-PHEMA-coated γ -Fe₂O₃, and (d) CPA-PVP-IBMB-coated γ -Fe₂O₃/PHEMA.

Table 5. Characteristics of γ -Fe₂O₃ Nanoparticles Coated with CPA-PVP-IBMB Macroinitiator and Polymerization of HEMA by “Grafting-from” Approach

	CPA-PVP-IBMB/ γ -Fe ₂ O ₃ (w/w)	D_n^a (nm)	PDI ^b	D_h^c (nm)	Z-potential (mV)	C (wt %)	N ^d (wt %)	Fe (wt %)	coating (wt %) based on		
									N	Fe	TGA
γ -Fe ₂ O ₃		11	1.15	125	-27	n.a.	n.a.	69.75	n.a.	n.a.	
CPA-PVP-IBMB-coated γ -Fe ₂ O ₃	2	19	1.13	196	-26	2.2	0.2	67.6	2.1	3.1	1.8
CPA-PVP-IBMB-coated γ -Fe ₂ O ₃ /PHEMA		21	1.15	652 ^e	-25	5.5	0.03	63.3	13.6	9.3	7.9

^a Number-average particle diameter (according to TEM). ^b Polydispersity index. ^c Hydrodynamic diameter. ^d Nitrogen analysis. ^e Particle sediment.

percentage of Fe in neat γ -Fe₂O₃. For example, AAS illustrated that the percentage of Fe was 67.6, thereby the calculated percentage of γ -Fe₂O₃ of the CPA-PVP-IBMB-coated γ -Fe₂O₃ nanoparticles was 96.9 wt %, i.e., percentage of coating was

3.1 wt % from AAS technique and 2.1 wt % according to the elemental analysis (0.2 wt % N; Table 5). The discrepancy could be caused by errors in the analysis. However, it can be assumed that the precursor macroinitiator was immobilized on the surface

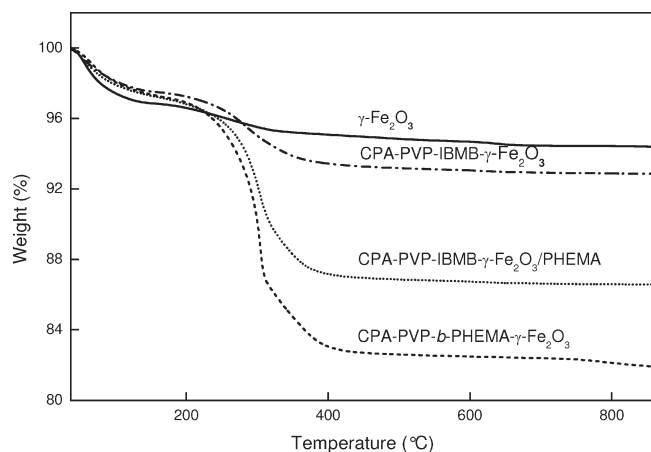


Figure 5. TGA thermographs of γ -Fe₂O₃, CPA-PVP-IBMB-coated γ -Fe₂O₃, CPA-PVP-IBMB-coated γ -Fe₂O₃/PHEMA, and CPA-PVP-*block*-PHEMA-coated γ -Fe₂O₃ nanoparticles.

of γ -Fe₂O₃ nanoparticles through physicochemical adsorption, namely, by the interaction between the γ -Fe₂O₃ surface with carboxyl group and vinylpyrrolidone chain of CPA-PVP-IBMB macroinitiator.

The CPA-PVP-IBMB content in the nanoparticles was determined also by thermogravimetric analysis of dried CPA-PVP-IBMB-coated γ -Fe₂O₃ nanoparticles, performed from room temperature to 800 °C (Figure 5). The CPA-PVP-IBMB-coated γ -Fe₂O₃ nanoparticles started losing weight at 150 °C, possibly because of the starting decomposition of CPA-PVP-IBMB macroinitiator, which then completely pyrolyzed at 400 °C. Determined weight loss of 1.8 wt % was roughly in agreement with the determination of coating from nitrogen analysis and by AAS.

The presence of immobilized CPA-PVP-IBMB macroinitiator on the surface of the γ -Fe₂O₃ nanoparticles was analyzed by ATR FT-IR spectroscopy. The infrared spectra of CPA-PVP-IBMB-coated γ -Fe₂O₃ nanoparticles, neat CPA-PVP-IBMB and neat γ -Fe₂O₃ were shown in Figure 6. The spectrum of CPA-PVP-IBMB-coated γ -Fe₂O₃ nanoparticles was very close to the spectrum of neat γ -Fe₂O₃ with additional weak bands at 1422 and 1285 cm⁻¹ coming from CPA-PVP-IBMB macroinitiator (Figure 6). The small blue shift and broadening of the band situated in the spectrum of γ -Fe₂O₃ at 1602 cm⁻¹ is most probably connected with the overlapping with C=O peak of VP units in CPA-PVP-IBMB macroinitiator and with its interaction with γ -Fe₂O₃ nanoparticles. ATR FT-IR spectroscopy thus confirmed that the γ -Fe₂O₃ nanoparticles were coated with CPA-PVP-IBMB macroinitiator.

TEM image of γ -Fe₂O₃ nanoparticles coated by CPA-PVP-*block*-PHEMA via “grafting-to” approach revealed that they were approximately of the same size (19 nm) like CPA-PVP-IBMB-coated nanoparticles (Figure 4 c). Hydrodynamic diameter of CPA-PVP-*block*-PHEMA-coated γ -Fe₂O₃ nanoparticles was 181 nm as determined by DLS, i.e., it increased compared with uncoated γ -Fe₂O₃ (Table 6). The increase of the polydispersity index (PDI = 1.48) and of hydrodynamic diameter in comparison with CPA-PVP-IBMB-coated nanoparticles reflect, in our opinion, formation of polymer shell around the magnetic core and clustering of the particles. However, the zeta-potential of CPA-PVP-*block*-PHEMA-coated nanoparticles (−28 mV) did not substantially change from that of neat γ -Fe₂O₃ indicating a good colloidal stability of the sample (Table 6). Moreover,

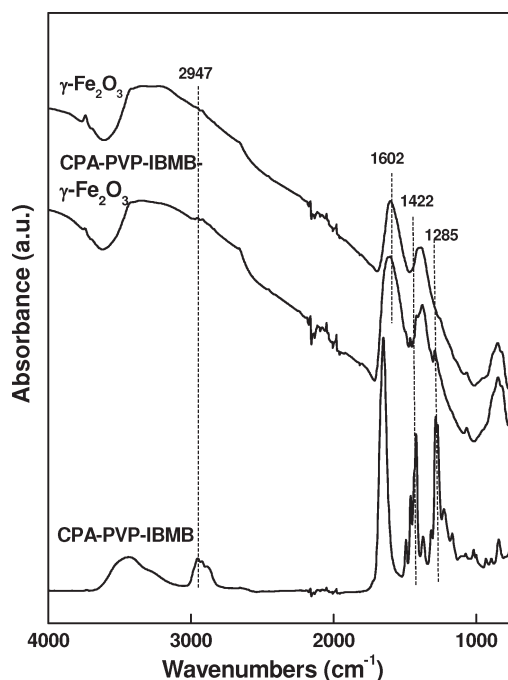


Figure 6. ATR FT-IR spectra of γ -Fe₂O₃ nanoparticles before and after coating with CPA-PVP-IBMB macroinitiator (CPA-PVP-IBMB/ γ -Fe₂O₃ ratio = 2 w/w).

0.2 wt % nitrogen and 62.7 wt % Fe were determined by elemental analysis and AAS, respectively, suggesting that 10.2 and 10.1 wt % coating was on the surface of the particles (Table 5). The amount of coating according to the thermogravimetric analysis of CPA-PVP-*block*-PHEMA-coated nanoparticles was only slightly higher (11.6 wt %). Three independent techniques revealed thus with a high accuracy the enhancement of the amount of the coating due to the increase of molecular weight of the immobilized CPA-PVP-*block*-PHEMA molecules (Table 6).

If the FT-IR spectrum of neat γ -Fe₂O₃ was compared with the spectrum of CPA-PVP-*block*-PHEMA-coated γ -Fe₂O₃, some additional peaks ascribed to CPA-PVP-*block*-PHEMA were observed (Figure 3). The spectrum was flat in the region of O–H and C–H stretching vibrations which may be connected with hydrogen bonding leading to the broadening and decreasing of the absorption in the region of O–H and C–H vibrations. It can be thus concluded that coating of γ -Fe₂O₃ with CPA-PVP-*block*-PHEMA copolymer was achieved.

More than two times higher packing density on γ -Fe₂O₃ nanoparticles was provided by CPA-PVP-IBMB macroinitiator than by CPA-PVP-*block*-PHEMA copolymer (Table 7) due to large number of CPA-PVP-IBMB chains occupying the same nanoparticle surface; overlapping polymer chains then enhanced the packing density. CPA-PVP-*block*-PHEMA copolymer thus occupied larger surface area and number of chains on one particle was lower compared with the macroinitiator.

Surface-Initiated Polymerization of HEMA on CPA-PVP-IBMB-Coated γ -Fe₂O₃ Nanoparticles. Macromolecular radicals from CPA-PVP-IBMB macroinitiator attached to the surface of γ -Fe₂O₃ nanoparticles were used to initiate polymerization of HEMA providing functionalization by “grafting-from” approach. The resulting CPA-PVP-IBMB-coated γ -Fe₂O₃/PHEMA particles were obtained at CPA-PVP-IBMB/ γ -Fe₂O₃ ratio = 2 (w/w). TEM of CPA-PVP-IBMB-coated γ -Fe₂O₃/PHEMA nanoparticles

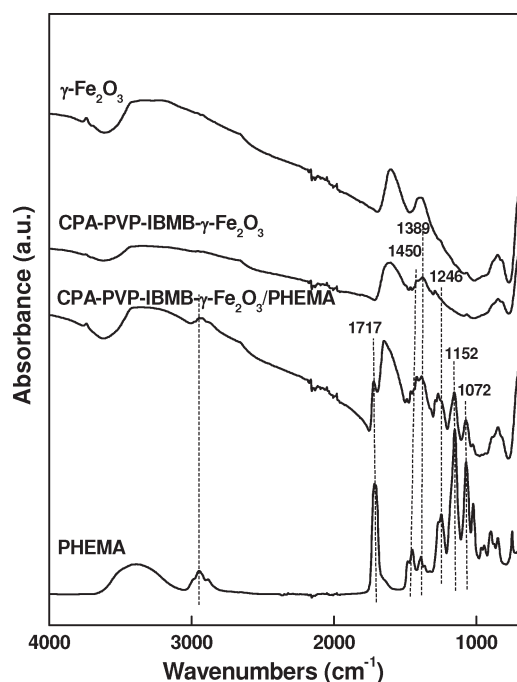
Table 6. Characteristics of γ -Fe₂O₃ Nanoparticles Coated with CPA-PVP-*block*-PHEMA by “Grafting-to” Approach

	CPA-PVP- <i>block</i> -PHEMA/ γ -Fe ₂ O ₃ (w/w)	D_n^a (nm)	PDI ^b	D_h^c (nm)	Z-potential (mV)	C (wt %)	N ^d (wt %)	Fe (wt %)	coating (wt %) based on		
									N	Fe	TGA
γ -Fe ₂ O ₃		11	1.15	168	-27	n.a.	n.a.	69.75	n.a.	n.a.	
CPA-PVP- <i>block</i> -PHEMA ^e -coated γ -Fe ₂ O ₃	2	19	1.48	181	-28	7.4	0.2	62.7	10.2	10.1	11.6

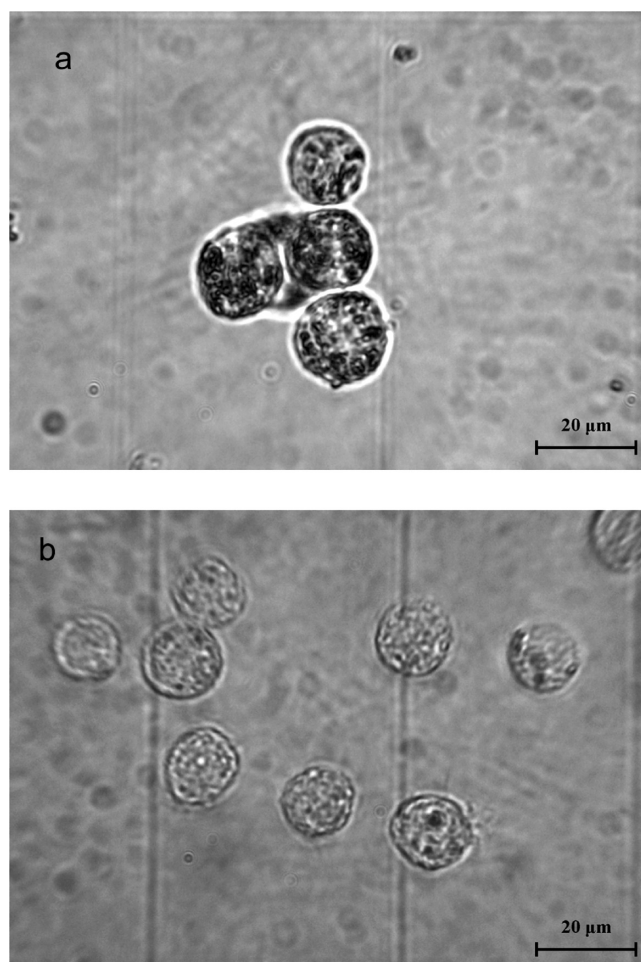
^a Number-average particle diameter (according to TEM). ^b Polydispersity index. ^c Hydrodynamic diameter. ^d Nitrogen analysis. ^e 2.15 wt % nitrogen in neat CPA-PVP-*block*-PHEMA.

Table 7. Characteristics of Particle Surface Area Modified by “Grafting-to” Approach

	D_n (nm)	polymer coating (wt %)	M_n polymer (kDa)	content of polymer (mol)	particle surface area (nm ²)	no. of polymer chains per particle	surface area covered by 1 molecule (nm ²)
CPA-PVP-IBMB-coated γ -Fe ₂ O ₃	19	2.1	17	2.26×10^{-23}	1134	13.6	83
CPA-PVP- <i>block</i> -PHEMA-coated γ -Fe ₂ O ₃	21	10.2	200	1.26×10^{-23}	1385	7.6	182

**Figure 7.** ATR FT-IR spectra of CPA-PVP-IBMB-coated γ -Fe₂O₃ nanoparticles before and after polymerization of HEMA; spectra of neat CPA-PVP-IBMB macroinitiator, PHEMA, and neat γ -Fe₂O₃ are shown as a control.

(Figure 4 d) revealed particle size \sim 21 nm with polydispersity characterized by PDI = 1.15. Both values did not substantially differ from CPA-PVP-IBMB-coated γ -Fe₂O₃ and CPA-PVP-*block*-PHEMA-coated γ -Fe₂O₃ nanoparticles. Hydrodynamic diameter of the particles determined by DLS was 652 nm suggesting both the increased chain length and its stretching in the medium as a result of high packing density of CPA-PVP-IBMB on the particle surface (Table 5). An amount of the polymer coating was very close to the value determined for the nanoparticles coated with block copolymers via “grafting-to” approach as $<$ 0.05 wt % of nitrogen and 63.3 wt % of Fe (Table 5) were found by elemental analysis and AAS, indicating that the amount of coating was 13.6 and 9.3 wt %, respectively.

**Figure 8.** Light micrographs of (a) fetal bovine serum opsonized CPA-PVP-IBMB-coated γ -Fe₂O₃/PHEMA nanoparticles phagocytosed by the murine macrophages J774.2 (0.025 wt % nanoparticles in medium) and (b) native macrophages J774.2 (control).

The polymer content in CPA-PVP-IBMB-coated γ -Fe₂O₃/PHEMA nanoparticles according to thermogravimetric analysis (Figure 5) was only slightly lower (7.9 wt %). The infrared

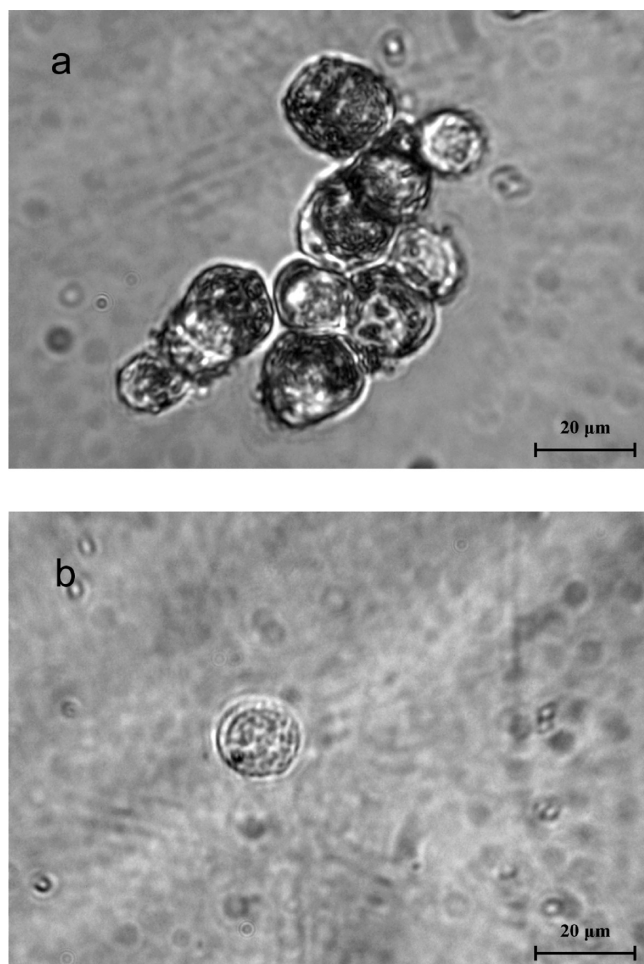


Figure 9. Light micrographs of (a) magnetically separated murine macrophages J774.2 that engulfed fetal bovine serum opsonized CPA-PVP-IBMB-coated γ -Fe₂O₃/PHEMA nanoparticles and (b) single macrophages J774.2 left in the culture medium after the magnetic separation. The macrophages were incubated in presence of the nanoparticles (0.025 wt %) for 24 h and then subjected to Dynal MPCTM-1 magnet.

spectrum of CPA-PVP-IBMB-coated γ -Fe₂O₃/PHEMA was compared with that of neat γ -Fe₂O₃, CPA-PVP-IBMA-coated particles and starting polymers (Figure 7). The spectrum of CPA-PVP-IBMB-coated γ -Fe₂O₃ (Figure 7) changed after the polymerization of HEMA. The most important peaks of PHEMA at 2947, 1716, 1450, 1389, 1246, 1152, and 1072 cm⁻¹ were well-detected in the spectrum of CPA-PVP-IBMB-coated γ -Fe₂O₃/PHEMA.

Phagocytosis of CPA-PVP-IBMB-coated γ -Fe₂O₃/PHEMA Nanoparticles by the Macrophages. Superparamagnetic CPA-PVP-IBMB-coated γ -Fe₂O₃/PHEMA nanoparticles were selected for the biological experiments, because they are expected to have relatively high packing density (similarly as CPA-PVP-IBMB-coated γ -Fe₂O₃ particles) compared with CPA-PVP-*block*-PHEMA-coated γ -Fe₂O₃ nanoparticles. CPA-PVP-IBMB-coated γ -Fe₂O₃/PHEMA and neat γ -Fe₂O₃ nanoparticles were compared in terms of *in vitro* targeting to murine monocytes/macrophages J774.2. The CPA-PVP-IBMB-coated γ -Fe₂O₃/PHEMA nanoparticles were first opsonized with fetal bovine serum proteins to facilitate their recognition by the phagocytic

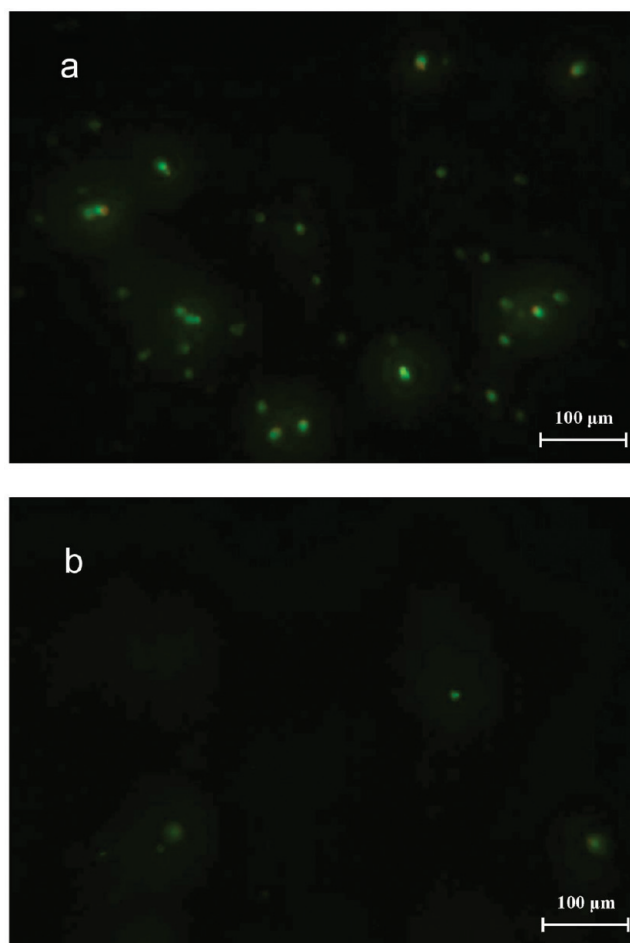
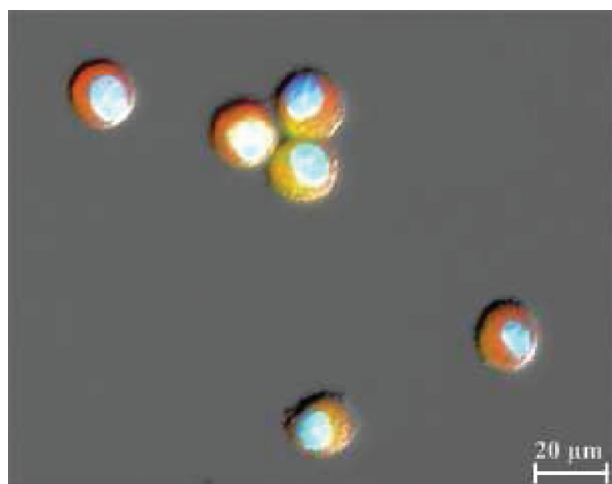
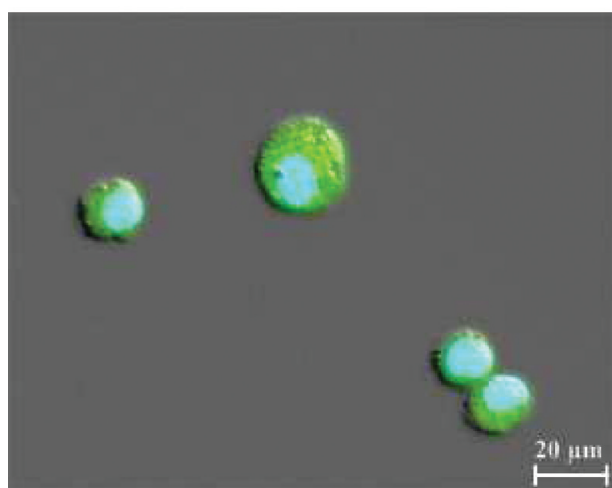


Figure 10. Fluorescence micrographs of acridine orange-stained (a) magnetically separated murine macrophages J774.2 that engulfed the fetal bovine serum opsonized CPA-PVP-IBMB-coated γ -Fe₂O₃/PHEMA nanoparticles and (b) single macrophages J774.2 left in the culture medium after the magnetic separation. The macrophages were incubated in presence of the nanoparticles (0.025 wt %) for 24 h and then subjected to the Dynal MPCTM-1 magnet.

cells. Both types of the nanoparticles were relatively nontoxic for cultured murine L1210 cells. Since the superparamagnetic CPA-PVP-IBMB-coated γ -Fe₂O₃/PHEMA nanoparticles were localized inside the macrophages (Figure 8a), the Dynal MPCTM-1 magnet separated the cells with engulfed nanoparticles from the particle-free cells (Figures 9 and 10). While magnetically separated macrophages contained many magnetic CPA-PVP-IBMB-coated γ -Fe₂O₃/PHEMA particles (Figure 9a), γ -Fe₂O₃ was absent in the cells remaining in the medium after the separation (Figure 9 b). Fluorescence microscopy confirmed that dominating part of the macrophages expressed their phagocytic activity and engulfed the protein-opsonized superparamagnetic CPA-PVP-IBMB-coated γ -Fe₂O₃/PHEMA nanoparticles (Figure 10). Maximal uptake of the particles was observed after 24 h incubation (time dependence of the uptake is not presented). It should be noted that neat γ -Fe₂O₃ nanoparticles were not only engulfed by the targeted macrophages but they activated them. In contrast, protein opsonized CPA-PVP-IBMB-coated γ -Fe₂O₃/PHEMA nanoparticles were engulfed by the macrophages not activating them (Figure 11). This was observed in fluorescence microscope after cell staining with acridine orange which is a lysosomotropic



a



b

Figure 11. Fluorescence micrographs of murine macrophages of J774.2 treated with (a) neat $\gamma\text{-Fe}_2\text{O}_3$ nanoparticles and (b) fetal bovine serum opsonized CPA-PVP-IBMB-coated $\gamma\text{-Fe}_2\text{O}_3$ /PHEMA nanoparticles. Cells were stained with acridine orange and Hoechst 33342. Red fluorescence seen distinctly only in cells that engulfed neat $\gamma\text{-Fe}_2\text{O}_3$ nanoparticles (a) is caused by the lysosomal activation. Blue fluorescence (Hoechst 33342) indicates nuclear chromatin in the cells.

weakly basic amino dye.^{65–67} In its stacked form, i.e., within lysosomes, acridine orange emits red fluorescence, whereas in the nuclei at neutral pH, it emits yellow-green. Activation of macrophages during the engulfment of foreign extracellular material is accompanied by an increase in the activity of digestive vacuoles, and thus, should cause red fluorescence shift due to accumulation of the dye in lysosomes.

The red fluorescence was intensified in most macrophages treated with neat $\gamma\text{-Fe}_2\text{O}_3$ nanoparticles, while only faint red fluorescence was expressed in single macrophages treated with the opsonized CPA-PVP-IBMB-coated $\gamma\text{-Fe}_2\text{O}_3$ /PHEMA nanoparticles (Figure 11). The opsonized nanoparticles looked thus to be more native for the macrophages compared with the neat $\gamma\text{-Fe}_2\text{O}_3$ nanoparticles. It is known that red fluorescence is characteristic for active lysosomal compartments which participate in the intracellular processing of the engulfed particles (microorganisms, viruses, damaged cells and foreign

macromolecules). Staining of cells with Hoechst 33342 allowed discriminating the nuclear material from the cytosolic one and demonstrated thus that red fluorescence was present only in the cytosolic area, where the lysosomes were located in cells.

The CPA-PVP-IBMB-PHEMA chains which easily conjugated proteins, made thus the CPA-PVP-IBMB-coated $\gamma\text{-Fe}_2\text{O}_3$ /PHEMA nanoparticles more native for the macrophages. Although the CPA-PVP-IBMB-coated $\gamma\text{-Fe}_2\text{O}_3$ /PHEMA nanoparticles were actively engulfed by the macrophages, the cells were not activated during phagocytosis. This fact is important if the newly developed superparamagnetic nanoparticles are engulfed by other cell types; such cells can be magnetically separated without a danger of adverse biochemical changes.

CONCLUSIONS

Two different approaches of functionalization of superparamagnetic $\gamma\text{-Fe}_2\text{O}_3$ nanoparticles were developed: “grafting-to” and “grafting-from” the particle surface using new heterotelechelic PVP peroxide with anchoring carboxyl group. First approach consisted in physicochemical adsorption of CPA-PVP-IBMB macroinitiator ($M_w \approx 17\,000$ Da) or CPA-PVP-*block*-PHEMA copolymer of high molecular weight (35 000 up to >200 000 Da) on $\gamma\text{-Fe}_2\text{O}_3$ surface using carboxyl end-group of heterotelechelic PVP peroxide. These nanoparticles did not substantially change D_n size from the uncoated particles. However, polydispersity of CPA-PVP-*block*-PHEMA-coated particles increased probably due to interactions of hydroxyl groups of the graft copolymer with the iron oxide surface. “Grafting-to” approach increased hydrodynamic size D_h to 180–200 nm (D_h of initial uncoated particles was 125 nm). Presence of coating on the particles was also confirmed by four independent techniques (FT-IR, TGA, AAS and elemental analysis). Coating of $\gamma\text{-Fe}_2\text{O}_3$ nanoparticles with CPA-PVP-IBMB lead to nanoparticles with compactly dense polymer shell. Second, “grafting-from”, approach involved initiation of polymerization of HEMA from the surface of CPA-PVP-IBMB-coated $\gamma\text{-Fe}_2\text{O}_3$ nanoparticles. This hydrodynamic diameter increased to 650 nm because of the increase of the length of chains attached to the particle surface and chain stretching in the medium.

Finally, superparamagnetic CPA-PVP-IBMB-coated $\gamma\text{-Fe}_2\text{O}_3$ /PHEMA nanoparticles were tested for phagocytosis by the macrophages and their subsequent magnetic separation. No irritation of living cells was observed and highly efficient engulfment of nanoparticles was confirmed. Magnetic separation of cells with engulfed CPA-PVP-IBMB-coated $\gamma\text{-Fe}_2\text{O}_3$ /PHEMA nanoparticles was easy and fast. Chemical properties of the heterotelechelic poly(*N*-vinylpyrrolidone) peroxide coating on the particle surface provide additional opportunity to attach different targeting and labeling molecules of potential biomedical significance, e.g., antibodies and lectins.

AUTHOR INFORMATION

Corresponding Author

*E-mail: horak@imc.cas.cz.

ACKNOWLEDGMENT

The authors thank Dr. P. Kadlec for static light scattering measurements. Financial support by the Grant Agency of the Czech Republic (203/09/1242 and P503/10/0664), the

Academy of Sciences of the Czech Republic (KAN401220801), and EU (NADINE Project 246513) is gratefully acknowledged.

REFERENCES

- (1) Tari, A.; Chantrell, R. W.; Charles, S. W.; Popplewell, J. *Phys. B* **1979**, *97*, 57–64.
- (2) Goldowsky, M. *IEEE Trans. Magn.* **1980**, *16*, 382–386.
- (3) Arbab, A. S.; Pandit, S. D.; Anderson, S. A.; Yocum, G. T.; Bur, M.; Frenkel, V.; Khuu, M. H.; Read, E. J.; Grank, J. A. *Stem Cells* **2006**, *24*, 671–678.
- (4) Lu, A. H.; Salabas, E. L.; Schüth, F. *Angew. Chem., Int. Ed.* **2007**, *46*, 1222–1244.
- (5) Tartaj, P.; Morales, M. P.; Gonzalez-Carreno, T.; Veintemillas-Verdaguer, S.; Serna, C. J. *J. Magn. Magn. Mater.* **2005**, *290*, 28–34.
- (6) Shubayev, V. I.; Pisanic, T. R.; Jin, S. *Adv. Drug Delivery Rev.* **2009**, *61*, 467–477.
- (7) Lee, J.; Lee, Y.; Youn, J. K.; Na, H. B.; Yu, T.; Kim, H.; Lee, S. M.; Koo, Y. M.; Kwak, J. H.; Park, H. G.; Chang, H. N.; Hwang, M.; Park, J. G.; Kim, J.; Hyeon, T. *Small* **2008**, *4*, 143–152.
- (8) Shamim, N.; Hong, L.; Hidajat, K.; Uddin, M. S. *Sep. Purif. Technol.* **2007**, *53*, 164–170.
- (9) Liu, L. H.; Dietsch, H.; Schurtenberger, P.; Yan, M. *Bioconjugate Chem.* **2009**, *20*, 1349–1355.
- (10) Kang, S. M.; Choi, I. S.; Lee, K. B.; Kim, Y. *Macromol. Res.* **2009**, *17*, 259–264.
- (11) Guo, S.; Dong, S. *Trends Anal. Chem.* **2009**, *28*, 96–109.
- (12) Yang, P.; Quan, Z.; Hou, Z.; Li, C.; Kang, X.; Cheng, Z.; Lin, J. *Biomaterials* **2009**, *30*, 4786–4795.
- (13) Pankhurst, Q. A.; Thanh, N. K. T.; Jones, S. K.; Dobson, J. *J. Phys. D, Appl. Phys.* **2009**, *42*, 224001–224015.
- (14) Guo, S.; Li, D.; Zhang, L.; Li, J.; Wang, E. *Biomaterials* **2009**, *30*, 1881–1889.
- (15) Butoescu, N.; Seemayer, C. A.; Palmer, G.; Guerne, P. A.; Gabay, C.; Doelker, E.; Jordan, O. *Arthritis Res. Ther.* **2009**, *11*, R72.
- (16) Jordan, A.; Scholz, R.; Maier-Hauff, K.; Johannsen, M.; Wust, P.; Nadobny, J.; Schirra, H.; Schmidt, H.; Deger, S.; Loening, S.; Lanksch, W.; Felix, R. *J. Magn. Magn. Mater.* **2001**, *225*, 118–126.
- (17) Herrera, A. P.; Rodriguez, M.; Torres-Lugo, M.; Rinaldi, C. *J. Mater. Chem.* **2008**, *18*, 855–858.
- (18) Lee, E. S. M.; Shuter, B.; Chan, J.; Chong, M. S. K.; Ding, J.; Teoh, S. H.; Beuf, O.; Briguot, A.; Tam, K. C.; Choolani, M.; Wang, S. C. *Biomaterials* **2010**, *31*, 3296–3306.
- (19) Yezhelyev, M.; Yacoub, R.; O'Regan, R. *Nanomedicine* **2009**, *4*, 83–103.
- (20) Kim, M. J.; Choa, Y. H.; Kim, D. H.; Kim, K. H. *IEEE Trans. Magn.* **2009**, *45*, 2446–2449.
- (21) Sun, C.; Lee, J. S. H.; Zhang, M. Q. *Adv. Drug Delivery Rev.* **2008**, *60*, 1252–1265.
- (22) Tiefenauer, L. X. In *Nanotechnology in Biology and Medicine: Methods, Devices, and Applications*; Vo-Dinh, T., Ed.; CRC Press: Boca Raton, FL, 2007; Chapter 29, pp 1–20.
- (23) Theppaleak, T.; Tumcharern, G.; Wichai, U.; Rutnakornpituk, M. *Polym. Bull.* **2009**, *63*, 79–90.
- (24) Kawaguchi, T.; Hanaichi, T.; Hasegawa, M.; Maruno, S. *J. Mater. Sci., Mater. Med.* **2001**, *12*, 121–127.
- (25) Chan, H. T.; Do, Y. Y.; Huang, P. L.; Chien, P. L.; Chan, T. S.; Liu, R. S.; Huang, C. Y.; Yang, S. Y.; Horng, H. E. *J. Magn. Magn. Mater.* **2006**, *304*, e415–e417.
- (26) Gupta, A. K.; Gupta, M. *Biomaterials* **2005**, *26*, 3995–4021.
- (27) Barrera, C.; Herrera, A. P.; Rinaldi, C. *J. Colloid Interface Sci.* **2009**, *329*, 107–113.
- (28) Yang, S.; Liu, H. R.; Zhang, Z. C. *J. Polym. Sci., Part A: Polym. Chem.* **2008**, *46*, 3900–3910.
- (29) Qian, Z.; Zhang, Z. C.; Chen, Y. J. *Colloid Interface Sci.* **2008**, *327*, 354–361.
- (30) Luo, Y. D.; Dai, C. A.; Chiu, W. Y. *J. Polym. Sci., Part A: Polym. Chem.* **2008**, *46*, 1014–1024.
- (31) Zhao, B.; Brittain, W. J. *Prog. Polym. Sci.* **2000**, *125*, 677–710.
- (32) Edmondson, S.; Osborne, V. L.; Huck, W. T. S. *Chem. Soc. Rev.* **2004**, *33*, 14–22.
- (33) Radhakrishnan, B.; Ranjan, R.; Brittain, W. J. *Soft Matter* **2006**, *2*, 386–396.
- (34) Zhou, Q.; Wang, S.; Fan, X.; Advincula, R.; Mays, J. *Langmuir* **2002**, *18*, 3324–3331.
- (35) Spange, S. *Prog. Polym. Sci.* **2000**, *25*, 781–849.
- (36) Eismann, U.; Spange, S. *Macromolecules* **1997**, *30*, 3439–3446.
- (37) Zirbs, R.; Binder, W.; Gahleitner, M.; Machl, D. *Macromol. Symp.* **2007**, *254*, 93–96.
- (38) Carrot, G.; Rutot-Houze, D.; Pottier, A.; Degee, P.; Hilborn, J.; Dubois, P. *Macromolecules* **2002**, *35*, 8400–8404.
- (39) Yoon, K. R.; Lee, Y. W.; Lee, J. K.; Choi, I. S. *Macromol. Rapid Commun.* **2004**, *25*, 1510–1513.
- (40) Joubert, M.; Delaite, C.; Bourgeat-Lami, E.; Dumas, P. *J. Polym. Sci., Part A: Polym. Chem.* **2004**, *42*, 1976–1984.
- (41) Tian, J.; Feng, Y. K.; Xu, Y. S. *Macromol. Res.* **2006**, *14*, 209–213.
- (42) Wang, L.; Neoh, K. G.; Kang, E. T.; Shuter, B.; Wang, S.-C. *Adv. Funct. Mater.* **2009**, *19*, 2615–2622.
- (43) Mingotaud, A. F.; Reculosa, S.; Mingotaud, C.; Keller, P.; Sykes, C.; Duguet, E.; Ravaine, S. *J. Mater. Chem.* **2003**, *13*, 1920–1925.
- (44) Jordi, M. A.; Seery, T. A. P. *J. Am. Chem. Soc.* **2005**, *127*, 4416–4422.
- (45) Kaiser, A.; Dutz, S.; Schmidt, A. M. *J. Polym. Sci., Part A: Polym. Chem.* **2009**, *47*, 7012–7020.
- (46) Vivek, A. V.; Dhamodharan, R. *J. Polym. Sci., Part A: Polym. Chem.* **2007**, *45*, 3818–3832.
- (47) Garcia, I.; Zafeiropoulos, N. E.; Janke, A.; Tercjak, A.; Eceiza, A.; Stamm, M.; Mondragon, I. *J. Polym. Sci., Part A: Polym. Chem.* **2007**, *45*, 925–932.
- (48) Binder, W. H.; Gloger, D.; Weinstabl, H.; Allmaier, G.; Pittenauer, E. *Macromolecules* **2007**, *40*, 3097–3107.
- (49) Cao, Y.; Ren, J.; Li, J.; Liu, Y. *Mater. Lett.* **2010**, *64*, 1570–1573.
- (50) Novikov, V.; Zaichenko, A.; Mitina, N.; Shevchuk, O.; Raevska, K.; Lobaz, V.; Lubenets, V.; Lastukhin, Y. *Macromol. Symp. (React. Polym.)* **2003**, *210*, 193–202.
- (51) Lukin, Yu. A.; Bakharev, V. I.; Zaichenko, A. S.; Voronov, S. A.; Zubov, V. P.; Gritskova, I. A.; Pravednikov, A. N. *Dokl. Akad. Nauk* **1985**, *285*, 155–161.
- (52) Zaichenko, A.; Mitina, N.; Shevchuk, O.; Rayevska, K.; Lobaz, V.; Skorokhoda, T.; Stoika, R. *Pure Appl. Chem.* **2008**, *80*, 2309–2326.
- (53) Zaichenko, A.; Mitina, N.; Shevchuk, O.; Shapoval, O.; Boiko, N.; Bilyy, R.; Stoika, R.; Voloshinovskii, A.; Horak, D. *AIP Conf. Proc.* **2010**, *1275*, 178–182.
- (54) Samaryk, V. Ya.; Varvarenko, S. M.; Zaichenko, O. S.; Nosova, N. G.; Roiter, Yu. V.; Mitina, N. E.; Gevus, O. I.; Tarnavchik, I. T. *Rep. Natl. Acad. Sci. Ukr.* **2002**, *12*, 118–123.
- (55) Bratychak, M. M.; Samarik, V. Ya.; Varvarenko, S. M.; Roiter, Yu. V.; Nosova, N. G.; Zaichenko, O. S.; Brostow, W. *Ukrainian Patent* 2003 56 799 A, 2003.
- (56) Skorokhoda, T. Ph.D. Thesis, Lviv National Polytechnic University, Lviv, Ukraine, 2009.
- (57) Sgouras, D.; Duncan, R. *J. Mater. Sci., Mater. Med.* **1990**, *1*, 61–68.
- (58) Diky, M. A.; Puchin, V. A.; Voronov, S. A.; Tokarev, V. S.; Hevus, O. I. *Russ. J. Org. Chem.* **1981**, *17*, 353–355.
- (59) Diky, M. A.; Puchin, V. A.; Vayda, M. S. *Russ. J. Org. Chem.* **1975**, *11*, 1902–1907.
- (60) Braun, D.; Cherdron, H.; Rehahn, M.; Ritter, H.; Voit, B. *Polymer Synthesis: Theory and Practice – Fundamentals, Methods, Experiments*; Springer: Berlin, 2005.
- (61) Babič, M.; Horák, D.; Jendelová, P.; Glogarová, K.; Herynek, V.; Trchová, M.; Likavčanová, K.; Hájek, M.; Syková, E. *Bioconjugate Chem.* **2009**, *20*, 283–294.
- (62) Bamford, C. H.; Tipper, C. F. H. In *The Practice of Kinetics*; Elsevier, 1969; Vol. 1.
- (63) Fargere, T.; Abdennadher, M.; Delmas, M.; Boutevin, B. *Eur. Polym. J.* **1995**, *31*, 489–497.

- (64) Slaughter, B. V.; Khurshid, S. S.; Fischer, O. Z.; Khademhosseini, A.; Peppas, N. A. *Adv. Mater.* **2009**, *21*, 3307–3327.
- (65) Kusuzaki, K.; Murata, H.; Takeshita, H.; Hashiguchi, S.; Nozaki, T.; Emoto, K.; Ashihara, T.; Hirasawa, Y. *Anticancer Res.* **2000**, *20*, 971–975.
- (66) Traganos, F.; Darzynkiewicz, Z. *Methods Cell Biol.* **1994**, *41*, 185–194.
- (67) Olsson, G. M.; Roberg, K.; Rundquist, I. *Anal. Cell Pathol.* **1990**, *2*, 179–188.